Reflectance Based Edge Classification

Theo Gevers and Harro Stokman
Faculty of Mathematics & Computer Science, University of Amsterdam
Kruislaan 403, 1098 SJ Amsterdam, The Netherlands
E-mail: {gevers, stokman}@wins.uva.nl

Abstract

Discriminating edge types, based on their local surface reflectance properties, is useful for a number of applications such as object recognition, stereo vision and structure from motion, where similar edge types (e.g. material transitions) from two distinct images are used for image matching while discounting other "accidental" edge types (e.g. shadows and highlight transitions).

Because intensity-based edge detectors cannot distinguish between various transition types (that is whether the transition is due to material changes, shadows, abrupt surface orientation changes or highlights), in this paper, we aim at using color information to classify the physical nature of the edge.

Therefore, the effect of varying imaging circumstances is analyzed. From this analysis we present the color models $c_1c_2c_3$ and $l_1l_2l_3$. It is shown that $l_1l_2l_3$ varies with a change in material only, $c_1c_2c_3$ with a change in material and highlights, and RGB vary with a change in material, highlights and geometry of an object. From these color models we derive gradient information which is used to classify edges in a color image to be one of the following types: (1) a shadow or geometry edge, (2) a highlight edge, (3) a material edge.

Experiments conducted with the edge classification technique on different color images show that the proposed method successfully discriminates the three different edge types.

keywords: image matching, color gradients, surface reflectance, color edge detection, color edge classification, photometric color invariants.

1 Introduction

Discriminating edge types, based on their local surface reflectance properties, is useful for a number of applications such as object recognition, stereo vision and structure from motion, where similar edge types (e.g. material transitions) from two distinct images are used for image matching while discounting other "accidental" edge types (e.g. shadows and highlight transitions).

The color (or rather, the apparent color) of an object varies with changes in illuminant color, illumination geometry (i.e. angle of incidence), viewing geometry (angle of reflectance), and miscellaneous sensor parameters. Consequently, the apparent color of an object can be different due to the varying imaging conditions.

Because intensity-based edge detectors cannot distinguish between different transition types, we use color information to classify the physical nature of a color edge. To this end, the effect of the varying imaging circumstances is analyzed. From this analysis, we derive color invariant gradient information which is used to classify edges in a color image to be one of the following types: (1) a shadow or geometry edge, (2) a highlight edge, (3) a material edge.

Different color edge detection schemes have been proposed. One of the first methods based on physics considerations is Klinker *et al.* [6] and Bajscy *et al.* [1]. Both methods retrieve "dog-leg" planar clusters in RGB-space yielding segmentation independent of the object's geometry, illumination conditions and highlights. Healey[5] proposes a method to segment images on the basis of normalized color. Recently, various color features have been studied using a multi-resolution segmentation method [7]. Although the above segmentation techniques are based on physics considerations to obtain segmentation results independent of the varying imaging conditions, they do not classify different color transitions in different transition types such as material changes, shadows, abrupt surface orientation changes or highlights. Therefore, in this paper, we propose a taxonomy for color invariance. The taxonomy is based upon the sensitivity of the different color models with respect to the following imaging conditions: object geometry, shadows, highlights, and material. From the taxonomy the edge classifier is derived.

The paper is organized as follows. In Section 2, color and reflection is discussed. In Section 3, different color models are presented. Then, in Section 4, we discuss the sensitivity of the different color models with respect to the imaging conditions. In Section 5, computational methods are proposed to compute color

invariant gradients. Next, in Section 6, the classification scheme is proposed to classify edges based on their local reflectance properties. Experiments carried out on a two color images are discussed in Section 4. Finally, several conclusions will be drawn.

2 Color and Reflection

Let $E(\vec{x}, \lambda)$ be the spectral power distribution of the incident (ambient) light at the object surface at $\vec{x}$, and let $L(\vec{x}, \lambda)$ be the spectral reflectance function of the object at $\vec{x}$. The spectral sensitivity of the kth sensor is given by $F_k(\lambda)$. Then ρ_k, the sensor response of the kth channel, is given by:

$$\rho_k(\vec{x}) = \int_\lambda E(\vec{x}, \lambda) L(\vec{x}, \lambda) F_k(\lambda) d\lambda \qquad (1)$$

where λ denotes the wavelength, and $L(\vec{x}, \lambda)$ is a complex function based on the geometric and spectral properties of the object surface. The integral is taken from the visible spectrum (e.g. 380-700 nm). Further, consider a opaque inhomogeneous dielectric object, then the geometric and surface reflection component in function $L(\vec{x}, \lambda)$ can be decomposed in a body and surface reflection component as described by Shafer [8]:

$$\phi_k(\vec{x}) = G_B(\vec{x}, \vec{n}, \vec{s}) \int_\lambda E(\vec{x}, \lambda) B(\vec{x}, \lambda) F_k(\lambda) d\lambda +$$

$$G_S(\vec{x}, \vec{n}, \vec{s}, \vec{v}) \int_\lambda E(\vec{x}, \lambda) S(\vec{x}, \lambda) F_k(\lambda) d\lambda \qquad (2)$$

giving the kth sensor response. For a color camera we have $k = \{R, G, B\}$. Further, $B(\vec{x}, \lambda)$ and $S(\vec{x}, \lambda)$ are the surface albedo and Fresnel reflectance at $\vec{x}$ respectively. $\vec{n}$ is the surface patch normal, $\vec{s}$ is the direction of the illumination source, and $\vec{v}$ is the direction of the viewer. Geometric terms G_B and G_S denote the geometric dependencies on the body and surface reflection component respectively.

Considering the neutral interface reflection (NIR) model (assuming that $S(\vec{x}, \lambda)$ has a constant value independent of the wavelength) and white illumination (approximately equal energy density for all wavelengths within the visible spectrum), then $S(\vec{x}, \lambda) = S(\vec{x})$, and $E(\vec{x}, \lambda) = E(\vec{x})$ and hence being constants (over the wavelengths). Then, we put forward that the measured sensor values are given by:

$$\omega_k(\vec{x}) = G_B(\vec{x}, \vec{n}, \vec{s}) E(\vec{x}) \int_\lambda B(\vec{x}, \lambda) F_k(\lambda) d\lambda +$$

$$G_S(\vec{x}, \vec{n}, \vec{s}, \vec{v}) E(\vec{x}) S(\vec{x}) \int_\lambda F_k(\lambda) d\lambda \qquad (3)$$

giving the kth sensor response of an infinitesimal surface patch under the assumption of a white light source.

If the integrated white condition holds (i.e. the area under the sensor spectral functions is approximately the same):

$$\int_\lambda F_i(\lambda) d\lambda = \int_\lambda F_j(\lambda) d\lambda \qquad (4)$$

we propose that the reflection from inhomogeneous dielectric materials under white illumination is given by:

$$\omega_k(\vec{x}) = G_B(\vec{x}, \vec{n}, \vec{s}) E(\vec{x}) \int_\lambda B(\vec{x}, \lambda) F_k(\lambda) d\lambda +$$

$$G_S(\vec{x}, \vec{n}, \vec{s}, \vec{v}) E(\vec{x}) S(\vec{x}) F \qquad (5)$$

If $\omega(\vec{x})$ is not dependent on $\vec{x}$, we obtain:

$$\omega_k = G_B(\vec{n}, \vec{s}) E \int_\lambda B(\lambda) F_k(\lambda) d\lambda +$$

$$G_S(\vec{n}, \vec{s}, \vec{v}) E S F \qquad (6)$$

This reflection model is used to study and analyze the subspace on which colors will be projected coming from the same uniformly colored surface.

3 Color Invariants

In this section, we discuss the different color models in Section 3.1 and their sensitivity with respect to the imaging conditions in Section 3.2. Finally, a taxonomy for color invariance is given which is used to classify edges on the basis of physics considerations.

3.1 Color models

In Gevers et al [3], [4] we have proposed different color models which some degree of invariance for the purpose of object recognition. The goal was to get more insight which color models to use under which imaging parameters. This is useful for object recognition applications where no constraints on the imaging process can be imposed as well as for applications where one or more parameters of the imaging process can be controlled such as for robots and industrial inspection (e.g. controlled object positioning and lightning conditions). For such a case, color models can be used for object recognition which are less invariant (at least under the given imaging conditions), but having higher discriminative power. In this paper, we use the different color models for the purpose of color edge classification. To that end, we focus on $c_1 c_2 c_3$ defined by [3], [4]:

$$c_1 = \arctan(\frac{R}{\max\{G, B\}}) \qquad (7)$$

$$c_2 = \arctan(\frac{G}{\max\{R,B\}}) \qquad (8)$$

$$c_3 = \arctan(\frac{B}{\max\{R,G\}}) \qquad (9)$$

and $l_1 l_2 l_3$ defined by [3], [4]:

$$l_1 = \frac{|R-G|}{|R-G|+|R-B|+|G-B|} \qquad (10)$$

$$l_2 = \frac{|R-B|}{|R-G|+|R-B|+|G-B|} \qquad (11)$$

$$l_3 = \frac{|G-B|}{|R-G|+|R-B|+|G-B|} \qquad (12)$$

In the next section, we discuss the sensitivity of $c_1 c_2 c_3$ and $l_1 l_2 l_3$ color models with respect to the imaging parameters.

3.2 Matte objects

Consider the body reflection term of Eq. (5):

$$\beta_k(\vec{x}) = G_B(\vec{x},\vec{n},\vec{s})E(\vec{x})\int_\lambda B(\vec{x},\lambda)F_k(\lambda)d\lambda \qquad (13)$$

giving the kth sensor response of an infinitesimal *matte* surface patch under the assumption of a white light source. Again, for a color camera, we have $k = \{R,G,B\}$.

According to the body reflection term, the color depends on $\int_\lambda B(\vec{x},\lambda)F_k(\lambda)d\lambda$ (i.e surface albedo and sensors) and the brightness on illumination intensity $E(\vec{x})$ and object geometry $G_B(\vec{x},\vec{n},\vec{s})$. A uniformly colored surface which is curved (i.e. varying surface orientation) gives rise to a broad variance of sensor values. Hence, RGB values obtained by a color camera will be negatively affected (color values will shift in RGB-color space) by the image-forming process. In contrast, we can prove that the $c_1 c_2 c_3$ color model, denoting the angles of the body reflection vector, is a color invariant for matte, dull objects cf. Eq. (13) and Eqs. (7) - (9):

$$c_1(\beta_R, \beta_G, \beta_B) =$$

$$\arctan(\frac{G_B(\vec{n},\vec{s})EK_R(\lambda)}{\max\{G_B(\vec{n},\vec{s})EK_G(\lambda), G_B(\vec{n},\vec{s})EK_B(\lambda)\}}) =$$

$$\arctan(\frac{K_R(\lambda)}{\max\{K_G(\lambda), K_B(\lambda)\}}) \qquad (14)$$

where

$$K_C(\lambda) = \int_\lambda B(\lambda)F_C(\lambda)d\lambda \text{ for } C \in \{R,G,B\} \qquad (15)$$

is the compact formulation depending on the sensors and surface albedo only. Equal arguments hold for c_1 and c_2. Note that the dependency on illumination, object pose, camera position, and object shape is factored out i.e. $c_1 c_2 c_3$ is only dependent on the sensors and the surface albedo.

Further, $l_1 l_2 l_3$ is a color invariant for matte objects as follows from substituting Eq. (13) in Eqs. (10) - (12):

$$l_1(\beta_R, \beta_G, \beta_B) =$$

$$\frac{G_B(\vec{n},\vec{s})E(|K_R(\lambda)-K_G(\lambda)|)}{G_B(\vec{n},\vec{s})E(|K_R(\lambda)-K_G(\lambda)|+|K_R(\lambda)-K_B(\lambda)|+|K_G(\lambda)-K_B(\lambda)|)} =$$

$$\frac{|K_R(\lambda)-K_G(\lambda)|}{|K_R(\lambda)-K_G(\lambda)|+|K_R(\lambda)-K_B(\lambda)|+|K_G(\lambda)-K_B(\lambda)|}$$

only dependent on the sensors and the surface albedo.

3.3 Shiny objects

Consider the surface reflection term of Eq. (5):

$$\gamma_k(\vec{x}) = G_S(\vec{x},\vec{n},\vec{s},\vec{v})E(\vec{x})S(\vec{x})F \qquad (16)$$

giving the kth sensor response for an infinitesimal *shiny* surface patch under white illumination.

Note that under the given conditions (NIR-model), the color of highlights is not related to the color of the surface on which they appear, but only on the color of the light source. Thus for the white light source, the measured values of a shiny surface can be represented by the surface reflection vector on the grey axis (i.e. main diagonal) of the sensor space. The extent of the highlight color cluster depends on the glossiness of the object surface.

For a given point on a shiny surface, the contribution of the body reflection component β and surface reflection component γ are added cf. Eq. (5). Consequently, $l_1 l_2 l_3$ is also independent of highlights as follows from substituting Eq. (5) in Eqs. (10) - (12):

$$l_1(\omega_R, \omega_G, \omega_B) =$$

$$\frac{|\beta_R-\beta_G|}{|\beta_R-\beta_G|+|\beta_R-\beta_B|+|\beta_G-\beta_B|}$$

$$\frac{G_B(\vec{n},\vec{s})E(|K_R(\lambda)-K_G(\lambda)|)}{G_B(\vec{n},\vec{s})E(|K_R(\lambda)-K_G(\lambda)|+|K_R(\lambda)-K_B(\lambda)|+|K_G(\lambda)-K_B(\lambda)|)} =$$

$$\frac{|K_R(\lambda)-K_G(\lambda)|}{|K_R(\lambda)-K_G(\lambda)|+|K_R(\lambda)-K_B(\lambda)|+|K_G(\lambda)-K_B(\lambda)|}$$

only dependent on the sensors and the surface albedo, where

$$K_k(\lambda) = \int_\lambda B(\lambda)F_k(\lambda)d\lambda \qquad (17)$$

is the compact formulation for the kth the channel.

3.4 Color invariant taxonomy

In the last section, the effect of varying imaging circumstances is analyzed. To achieve this, the dichromatic reflection model under white illumination has been studied. From this analysis it has been shown that $l_1 l_2 l_3$ varies with a change in material only, $c_1 c_2 c_3$ with a change in material and highlights, and RGB varies with a change in material, highlights and geometry of an object. The color invariance taxonomy is shown in Fig. 1. The taxonomy is based upon the sensitivity of the color models with respect to the following imaging conditions: object geometry, shadows, highlights, and material.

	object shape	shadows	highlights	material
RGB	+	+	+	+
c1c2c3	-	-	+	+
l1l2l3	-	-	-	+

Figure 1: *Taxonomy of color invariance based upon the sensitivity of the different color models with respect to the following imaging conditions: $l_1 l_2 l_3$ varies with a change in material only, $c_1 c_2 c_3$ with a change in material and highlights, and RGB varies with a change in material, highlights and geometry of an object. - denotes invariant and + denotes sensitivity of the color model to the*

In the remainder of the paper, the taxonomy will be used to classify edges in a color image to be one of the following types: (1) a shadow or geometry edge, (2) a highlight edge, (3) a material edge.

4 Color Invariant Gradients

In the previous section, color models are discussed which are invariant under varying imaging conditions. In this section, we present color invariant edges derived from the different color models.

4.1 Gradients in multi-valued images

In contrast to gradient methods which combine individual components of a multi-valued image in an ad hoc manner without any theoretical basis (e.g. taking the sum or RMS of the component gradient magnitudes as the magnitude of the resultant gradient), we follow the principled way to compute gradients in vector images as described by Silvano di Zenzo [9] and further used in [10], which is summarized as follows.

Let $\Theta(x_1, x_2) : \Re^2 \rightarrow \Re^m$ be a m-band image with components $\Theta_i(x_1, x_2) : \Re^2 \rightarrow \Re$ for $i = 1, 2, ..., m$.

For color images we have $m = 3$. Hence, at a given image location the image value is a vector in $\Re^m$. The difference at two nearby points $P = (x_1^0, x_2^0)$ and $Q = (x_1^1, x_2^1)$ is given by $\triangle \Theta = \Theta(P) - \Theta(Q)$. Considering an infinitesmall displacement, the difference becomes the differential $d\Theta = \sum_{i=1}^{2} \frac{\partial \Theta}{\partial x_i} dx_i$ and its squared norm is given by:

$$d\Theta^2 = \sum_{i=1}^{2} \sum_{k=1}^{2} \frac{\partial \Theta}{\partial x_i} \frac{\partial \Theta}{\partial x_k} dx_i dx_k = \sum_{i=1}^{2} \sum_{k=1}^{2} g_{ik} dx_i dx_k =$$

$$\begin{bmatrix} dx_1 \\ dx_2 \end{bmatrix}^T \begin{bmatrix} g_{11} & g_{12} \\ g_{21} & g_{22} \end{bmatrix} \begin{bmatrix} dx_1 \\ dx_2 \end{bmatrix} \qquad (18)$$

where $g_{ik} := \frac{\partial \Theta}{\partial x_i} \cdot \frac{\partial \Theta}{\partial x_k}$ and the extrema of the quadratic form are obtained in the direction of the eigenvectors of the matrix $[g_{ik}]$ and the values at these locations correspond with the eigenvalues given by:

$$\lambda_\pm = \frac{g_{11} + g_{22} \pm \sqrt{(g_{11} - g_{22})^2 + 4g_{12}^2}}{2} \qquad (19)$$

with corresponding eigenvectors given by $(\cos \theta_\pm, \sin \theta_\pm)$, where $\theta_+ = \frac{1}{2} \arctan \frac{2g_{12}}{g_{11} - g_{22}}$ and $\theta_- = \theta_+ + \frac{\pi}{2}$. Hence, the direction of the minimal and maximal changes at a given image location is expressed by the eigenvectors θ_- and θ_+ respectively, and the corresponding magnitude is given by the eigenvalues λ_- and λ_+ respectively. Note that λ_- may be different than zero and that the strength of an multi-valued edge should be expressed by how λ_+ compares to λ_-, for example by subtraction $\lambda_+ - \lambda_-$ as proposed by [10], which will be used to define gradients in multi-valued color *invariant* images in the next section.

4.2 Gradients in multi-valued color invariant images

In this section, we propose color invariant gradients based on the multi-band approach as described in the previous section.

The color gradient for RGB is as follows:

$$\nabla \mathcal{C}_{RGB} = \sqrt{\lambda_+^{RGB} - \lambda_-^{RGB}} \qquad (20)$$

for

$$\lambda_\pm = \frac{g_{11}^{RGB} + g_{22}^{RGB} \pm \sqrt{(g_{11}^{RGB} - g_{22}^{RGB})^2 + 4(g_{12}^{RGB})^2}}{2} \qquad (21)$$

where $g_{11}^{RGB} = |\frac{\partial R}{\partial x}|^2 + |\frac{\partial G}{\partial x}|^2 + |\frac{\partial B}{\partial x}|^2$, $g_{22}^{RGB} = |\frac{\partial R}{\partial y}|^2 + |\frac{\partial G}{\partial y}|^2 + |\frac{\partial B}{\partial y}|^2$, $g_{12}^{RGB} = \frac{\partial R}{\partial x} \frac{\partial R}{\partial y} + \frac{\partial G}{\partial x} \frac{\partial G}{\partial y} + \frac{\partial B}{\partial x} \frac{\partial B}{\partial y}$.

Further, we propose that the color invariant gradient (based on $c_1 c_2 c_3$) for matte objects is given by:

$$\nabla \mathcal{C}_{c_1 c_2 c_3} = \sqrt{\lambda_+^{c_1 c_2 c_3} - \lambda_-^{c_1 c_2 c_3}} \qquad (22)$$

for

$$\lambda_\pm = \frac{g_{11}^{c_1 c_2 c_3} + g_{22}^{c_1 c_2 c_3} \pm \sqrt{(g_{11}^{c_1 c_2 c_3} - g_{22}^{c_1 c_2 c_3})^2 + 4(g_{12}^{c_1 c_2 c_3})^2}}{2} \qquad (23)$$

where $g_{11}^{c_1 c_2 c_3} = |\frac{\partial c_1}{\partial x}|^2 + |\frac{\partial c_2}{\partial x}|^2 + |\frac{\partial c_3}{\partial x}|^2$, $g_{22}^{c_1 c_2 c_3} = |\frac{\partial c_1}{\partial y}|^2 + |\frac{\partial c_2}{\partial y}|^2 + |\frac{\partial c_3}{\partial y}|^2$, $g_{12}^{c_1 c_2 c_3} = \frac{\partial c_1}{\partial x}\frac{\partial c_1}{\partial y} + \frac{\partial c_2}{\partial x}\frac{\partial c_2}{\partial y} + \frac{\partial c_3}{\partial x}\frac{\partial c_3}{\partial y}$.

Similarly, we propose that the color invariant gradient (based on $l_1 l_2 l_3$) for shiny objects is given by:

$$\nabla \mathcal{C}_{l_1 l_2 l_3} = \sqrt{\lambda_+^{l_1 l_2 l_3} - \lambda_-^{l_1 l_2 l_3}} \qquad (24)$$

for

$$\lambda_\pm = \frac{g_{11}^{l_1 l_2 l_3} + g_{22}^{l_1 l_2 l_3} \pm \sqrt{(g_{11}^{l_1 l_2 l_3} - g_{22}^{l_1 l_2 l_3})^2 + 4(g_{12}^{l_1 l_2 l_3})^2}}{2} \qquad (25)$$

where $g_{11}^{l_1 l_2 l_3} = |\frac{\partial l_1}{\partial x}|^2 + |\frac{\partial l_2}{\partial x}|^2 + |\frac{\partial l_3}{\partial x}|^2$, $g_{22}^{l_1 l_2 l_3} = |\frac{\partial l_1}{\partial y}|^2 + |\frac{\partial l_2}{\partial y}|^2 + |\frac{\partial l_3}{\partial y}|^2$, $g_{12}^{l_1 l_2 l_3} = \frac{\partial l_1}{\partial x}\frac{\partial l_1}{\partial y} + \frac{\partial l_2}{\partial x}\frac{\partial l_2}{\partial y} + \frac{\partial l_3}{\partial x}\frac{\partial l_3}{\partial y}$.

In the next section, the color invariant gradients will be used to discriminate the different edge types by their physical nature.

5 Reflectance Based Edge Classification

In the previous section, the effect of varying imaging circumstances have been analyzed first for dichromatic reflectance under white illumination differentiated for RGB, $c_1 c_2 c_3$ and $l_1 l_2 l_3$. From the color invariance taxonomy and the computational techniques for gradient calculation, we may conclude that $\nabla \mathcal{C}_{RGB}$ measures the presence of (1) shadow or geometry edges, (2) highlight edges, (3) material edges. Further, $\nabla \mathcal{C}_{l_1 l_2 l_3}$ measures the presence of (2) highlight edges, (3) material edges. And $\nabla \mathcal{C}_{l_1 l_2 l_3}$ measures the presence of only (3) material edges. Similar to the color invariance taxonomy, a taxonomy of color edges can be given, see Fig. 2. The color edge taxonomy is based upon the sensitivity of the color gradients with respect to the following imaging conditions: object geometry, shadows, highlights, and material.

Based on the given color edge taxonomy, we now present a color edge classifier discriminating edges in one of the following types: (1) a shadow or geometry edge, (2) a highlight edge, (3) a material edge.

Let the set of image coordinates of local RGB edge maxima in image be denoted by E which will be zero

	shape edges	shadow edges	highlight edges	material edges
$\blacktriangledown C_{RGB}$	+	+	+	+
$\blacktriangledown C_{c1c2c3}$	-	-	+	+
$\blacktriangledown C_{l1l2l3}$	-	-	-	+

Figure 2: *Taxonomy of color edges based upon the sensitivity of the different color models with respect to the following imaging conditions. - denotes invariant and + denotes sensitivity of the color model to the*

except at RGB edges. To find RGB edges in images we use the Canny-edge detector with non-maximum suppression applied on $\nabla \mathcal{C}_{RGB}$. Then the rule-based reflectance classifier is as follows:

IF $(\nabla \mathcal{C}_{RGB}) > t_1$ AND $(\nabla \mathcal{C}_{c_2 c_3}) \leq t_2$
THEN classify as **shadow or geometry edge**
ELSE
IF $(\nabla \mathcal{C}_{c_1 c_2 c_3}) > t_2$ AND $(\nabla \mathcal{C}_{l_1 l_2 l_3}) \leq t_3$
THEN classify as **highlight edge**
ELSE
IF $(\nabla \mathcal{C}_{l_1 l_2 l_3}) > t_3$
THEN classify as **material edge**

only computed for $\vec{x} \in E$ that is only at a RGB edge maximum. Further, t_i are thresholds based on the noise level to suppress marginally visible edges.

6 Experiments

6.1 The first recording

.

Figure 4.a is an image of several toys against a background consisting of four squares. The size of the image is 256x256. The first upper left quadrant consists of three homogeneously painted matte cubes of wood. The second upper right quadrant contains two specular plastic donuts on top of each other. In the bottom left quadrant a red highlighted ball and a matte cube are shown while the last quadrant contains two matte cubes. The image is clearly contaminated by shadows, shading, highlights and inter-reflections. Inter-reflections occur when an object receives the reflected light from other objects. Note that each individual object is painted homogeneously with a distinct color.

In Figure 3.a edges are shown obtained from the RGB image. Clearly, edges are introduced by abrupt surface orientations, shadows, inter-reflections and highlights. In contrast, computed edges for $c_1 c_2 c_3$ and $l_1 l_2 l_3$ defined by $\nabla \mathcal{C}_{c_1 c_2 c_3}$ and $\nabla \mathcal{C}_{l_1 l_2 l_3}$ respectively, shown in Figure 3.b and 3.c, are insensitive for shad-
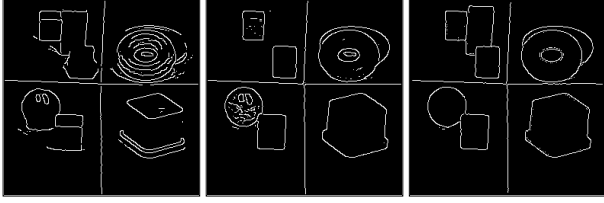
Figure 3: *Edge maps of the various color models computed from the first recorded color image shown in Figure 4.a. a. Edge map based on RGB gradient field $\nabla \mathcal{C}_{RGB}$ with non-maximum suppression. b. Edge map based on $c_1 c_2 c_3$ gradient field $\nabla \mathcal{C}_{c_1 c_2 c_3}$ with non-maximum suppression. c. Edge map based on $l_1 l_2 l_3$ gradient field $\nabla \mathcal{C}_{l_1 l_2 l_3}$ with non-maximum suppression.*

ows and surface orientation changes. In Figure 3.c the edge map is shown for $l_1 l_2 l_3$ with non-maximum suppression. Good performance is shown where computed edges correspond to material boundaries discounting the disturbing influences of surface orientation, illumination, shadows and highlights. Only inter-reflections disturb the quality of the edge map slightly (note that $l_1 l_2 l_3$ is not robust to inter-reflections).

The results of the proposed reflectance based edge classifier are shown in Figure 4.b for the color image shown in Figure 4.a. The edge classifier discriminates edges in the color image to be one of the following types: (1) a shadow or geometry edge shown in Figure 4.c, (2) a highlight edge shown in Figure 4.d, (3) a material edge shown in Figure 4.e. From the observed results, the edge classifier discriminates the three edge types successfully. Only minor performance is achieved when intensity and highlights change smoothly over a wide image range due to the local behavior of the edge classifier.

6.2 The second recording

.

In Figure 6.a, the second recorded full-color image is shown containing various rigid objects against a uniform background. The size of the image is 256x256. In the first quadrant, two cubes of painted wood are shown. The second quadrant contains a plastic cup and in the third quadrant a highlighted plastic donut is shown. The right-bottom quadrant consists of two cubes. Again, the image is affected by shadows, shading, highlights and inter-reflections. Each object is painted uniformly with a distinct color.

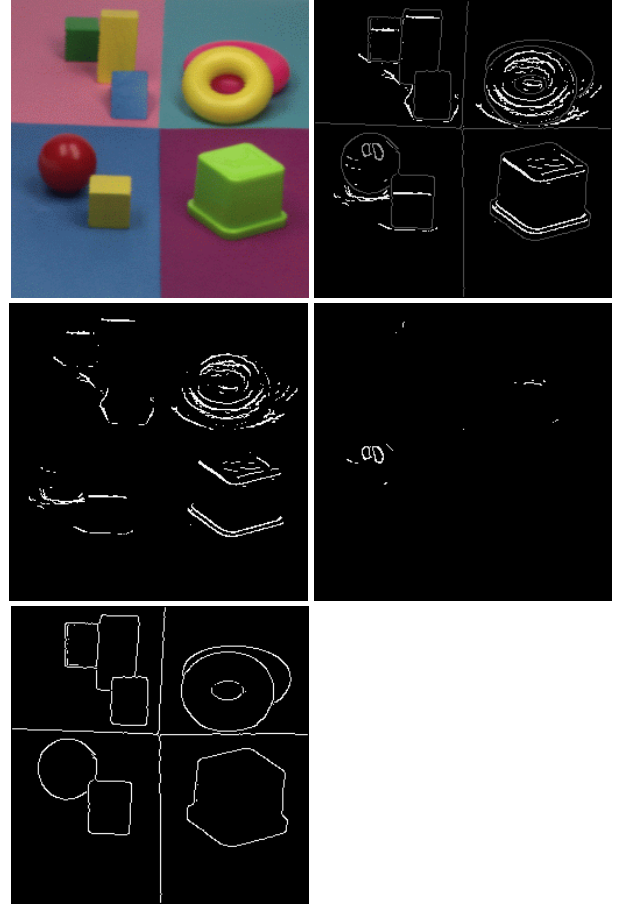Accidental edges computed from *RGB*, depicted in

Figure 4: *a. First recorded color image. b. Reflectance based edge classification. c. shadow and geometry edges d. highlight edges e. material transition.*

Figure 5.a, are introduced due to shadows (e.g. casted by the cubes upon the background), abrupt surface orientation (e.g. the cup), inter-reflections (e.g. donut and background) and highlights (e.g. the highlighted donut). These edges do not correspond to material transitions. $c_1 c_2 c_3$ yields an edge map which is fairly independent of shadows and abrupt surface orientation changes but erroneous edges are generated by image noise and small specularities due to local variations in material composition of objects and highlights. In contrast, good performance is shown for $l_1 l_2 l_3$ as depicted in 5.c except for the disturbing effects of image noise and variations in material composition.

Results of the edge classifier are shown in Figure 6.b for the color image shown in Figure 6.a. The edge classifier successfully discriminates edges in the color image to be one of the following types: (1) a shadow
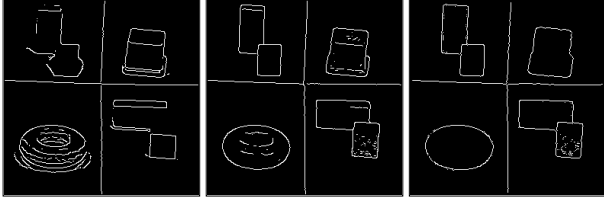
Figure 5: *Edge maps of the various color models computed from the first recorded color image shown in Figure 6.a. a. Edge map based on RGB gradient field $\nabla \mathcal{C}_{RGB}$ with non-maximum suppression. b. Edge map based on $c_1 c_2 c_3$ gradient field $\nabla \mathcal{C}_{c_1 c_2 c_3}$ with non-maximum suppression. c. Edge map based on $l_1 l_2 l_3$ gradient field $\nabla \mathcal{C}_{l_1 l_2 l_3}$ with non-maximum suppression.*

or geometry edge shown in Figure 6.c, (2) a highlight edge shown in Figure 6.d, (3) a material edge shown in Figure 6.e. Again minor performance is achieved when intensity and highlights change smoothly over a wide image range.

7   Conclusion

Because intensity-based edge detectors cannot distinguish between various transition types (that is whether the transition is due to material changes, shadows, abrupt surface orientation changes or highlights), in this paper, we aim at using color information to classify the physical nature of the edge.

In theory, the effect of varying imaging circumstances are analyzed. From this analysis we present the color models $c_1 c_2 c_3$ and $l_1 l_2 l_3$. It is shown that $l_1 l_2 l_3$ varies with a change in material only, $c_1 c_2 c_3$ with a change in material and highlights, and RGB vary with a change in material, highlights and geometry of an object. From these color models we derive gradient information which is used to classify edges in a color image to be one of the following types: (1) a shadow or geometry edge, (2) a highlight edge, (3) a material edge.

Experiments conducted with the edge classification technique on different color images show that the proposed method successfully discriminates the four different edge types.

No constraints have been imposed on the images and the camera image process other than that images should be taken from chromatic objects illuminated by average day-light color. It is our point of view that these conditions are acceptable for a large variety of applications yielding a promising reflectance based edge
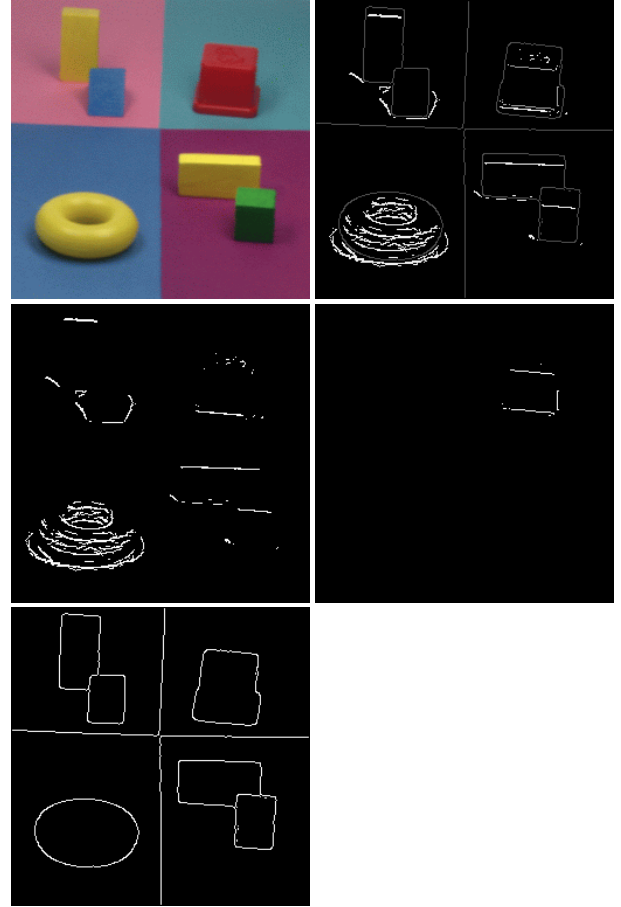

Figure 6: *a. Second recorded color image. b. Reflectance based edge classification. c. shadow and geometry edges d. highlight edges e. material transition.*

classifier for images from real world scenes.

References

[1] Bajcsy, R., Lee S. W., and Leonardis, A., *Color Image Segmentation with Detection of Highlights and Local Illumination Induced by Interreflections*, In IEEE 10th ICPR'90, pp. 785-790, Atlantic City, NJ, 1990.

[2] Canny, J., *A Computational Approach to Edge Detection*, IEEE Transactions on Pattern Analysis and Machine Intelligence, Vol. 8, No. 6, pp. 679-698, 1986.

[3] Gevers, T and Smeulders W.M., *Color Based Object Recognition*, Pattern Recognition, 32, pp. 453-464, 1999.

[4] Gevers, T. and Smeulders W.M., *Color Invariant Snakes*, BMVC98, Southampton, 1998.

[5] Healey, G., *Segmenting Images Using Normalized Color*, IEEE Syst., Man. Cybern., Vol. 22, pp. 64-73, 1992.

[6] Klinker, G. J., Shafer, A. and Kanada, T. *A Physical Approach to Color Image Understanding*, Int. J. of Comp. Vision, Vol. 4, pp. 7-38, 1990.

[7] Liu, J. and Yang, Y-H., *Multi-resolution Color Image Segmentation*, IEEE PAMI, Vol. 16, No. 7, pp. 689-700, 1994.

[8] Shafer, S. A., *Using Color to Separate Reflection Components*, COLOR Res. Appl., 10(4), pp 210-218, 1985.

[9] S. di Zenzo, *Gradient of a Multi-images*, CVGIP, 33:116-125, 1986.

[10] G. Sapiro, D. L. Ringach, *Anisotropic Diffusion of Multi-valued Images with Applications*, to Color Filtering, IEEE PAMI, (5)11, 1582-1586, 1996.